(This is a sample cover image for this issue. The actual cover is not yet available at this time.)

Earth and Planetary Science Letters 337–338 (2012) 17–24

Contents lists available at SciVerse ScienceDirect

Earth and Planetary Science Letters

journal homepage: www.elsevier.com/locate/epsl

An iron isotope perspective on the origin of the nanophase metallic iron in lunar regolith

Kun Wang*, Frédéric Moynier, Frank A. Podosek, Julien Foriel

Department of Earth and Planetary Sciences and McDonnell Center for the Space Sciences, Washington University in St Louis, One Brookings Drive, St Louis, MO 63130, USA

ARTICLE INFO

Article history:
Received 12 December 2011
Received in revised form
16 April 2012
Accepted 16 May 2012
Editor: T. Elliot

Keywords:
Iron isotopes
nanophase metallic iron
space weathering
lunar regolith
the moon

ABSTRACT

The surfaces of the Moon and other airless planetary bodies are constantly weathered by meteorite impacts and sputtering by charged particles. One of the hallmarks of this "space weathering" is the presence of nanophase metallic Fe ($npFe^0$) at the surface of airless bodies. These $npFe^0$ grains alter the surface optical spectra of planetary bodies without an atmosphere and their concentration is used to estimate the degree of maturity of lunar regolith. The origin of $npFe^0$ has been debated between in situ reduction due to the solar wind, and evaporation generated by charged particle sputtering and/or micrometeorite impact followed by re-condensation of metallic Fe. These two mechanisms will impart completely different Fe isotopic fractionation effects on the $npFe^0$. In this study we measure the Fe isotopic composition of $npFe^0$ using a step-by-step surface etching technique on lunar regolith plagioclase. Our results show that $npFe^0$ is highly enriched in the heavy isotopes of Fe (δ^{56}Fe up to 0.71‰) compared to bulk plagioclase and other lunar materials such as regolith and igneous rocks. We suggest that the formation of $npFe^0$ in lunar regolith is responsible for the higher δ^{56}Fe in the lunar regolith compared to lunar igneous rocks. In addition, a thermal escape model shows that the heavy Fe isotopic composition of $npFe^0$ is best explained by the preferential escape of light Fe isotopes to space in the vaporization phase of Fe. The temperature of the vapor can be inferred from our model (2750–3000 K), which is compatible with those proposed by previous calculations and experiments. Therefore our results unambiguously support the vapor deposit origin of $npFe^0$, explain the origin of the heavy Fe isotopic composition of the lunar regolith and provide a temperature estimate for the impact event at the origin of the $npFe^0$.

1. Introduction

The Moon, as well as other small terrestrial bodies like Phobos and 4-Vesta have little to no atmosphere or magnetic field. All planetary bodies are under continuous bombardment by various events such as cosmic ray radiation, solar wind sputtering/implantation, and meteorite/micrometeorite impacts (Clark et al., 2002; Lucey et al., 2006). While both the atmosphere and magnetic field protect the Earth from the majority of these effects, these processes constantly alter the unprotected surface of airless bodies and/or the bodies absent of significant magnetic fields. The cumulative alteration effects of these events are loosely defined as "space weathering" (Hapke, 2001; Pieters et al., 2000). On these airless planetary bodies, space weathering has long been recognized as a key factor for the alteration of surface optical features by, for example, lowering the albedo, reddening the spectral slope, and subduing the absorption fine structures (Adams and Jones, 1970; Clark et al., 2002; Hapke, 2001). Space weathering complicates the interpretation of the composition of airless bodies' surface materials (Chapman, 2004; Clark et al., 2002) and makes it almost impossible to spectrally match groups of meteorites with types of asteroids (Britt et al., 1992).

Lunar regolith samples provide the best available materials to study space weathering, and the knowledge learned about space weathering from these samples could be extended to other airless bodies (Taylor et al., 2001). Nanophase metallic Fe ($npFe^0$) is widely observed on the surface of lunar regolith minerals or inside agglutinates (Keller and McKay, 1993, 1997; Wentworth et al., 1999), and it has been thought to be the cause of alteration of optical spectra from the lunar surface (Hapke et al., 1975; Moroz et al., 1996; Sasaki et al., 2001; Tang et al., 2011). Understanding the origin and characteristics of $npFe^0$ is critical to the interpretation of remote sensing data from the Moon and other airless planetary bodies. In addition, the characteristic ferromagnetic resonance of $npFe^0$ has been used as the main index to evaluate the maturity of the lunar regolith (Cirlin et al., 1974; Housley et al., 1975; Morris, 1976; Pearce et al., 1974).

* Corresponding author.
E-mail addresses: wangkun@wustl.edu (K. Wang), moynier@levee.wustl.edu (F. Moynier), fap@levee.wustl.edu (F.A. Podosek), foriel@levee.wustl.edu (J. Foriel).

0012-821X/$ - see front matter © 2012 Elsevier B.V. All rights reserved.
http://dx.doi.org/10.1016/j.epsl.2012.05.021

Therefore understanding the origin and formation mechanism of $npFe^0$ is also very important for explaining the exposure history of lunar regolith.

After the discovery of $npFe^0$ on the surface of lunar regolith grains and inside agglutinates, two competing theories were proposed to explain its origin. The first and long-accepted one is that $npFe^0$ is formed as the reduction of silicates/oxide in lunar regolith saturated with solar-wind-implanted hydrogen during impact melting (Housley et al., 1973). Concurrently, it was suggested that $npFe^0$ was actually formed as the deposition of the solar wind sputtering/micrometeorite impact-generated vapors (Hapke, 1973; Hapke et al., 1975).

The model of Housley et al. (1973) was widely accepted. It is, however, problematic because (1) the reduction process would have formed by-product water ($FeO+2H=Fe+H_2O\uparrow$), and the presence of water in lunar regolith is still not fully accepted (Taylor et al., 1995). Although many recent studies have described the detection of OH/H_2O at the lunar surface, the source of water (indigenous, solar wind reduction, or meteoritic component) remains largely unknown (Clark, 2009; Liu et al., 2012; Pieters et al., 2009; Sunshine et al., 2009); (2) pulse laser irradiation experiments, simulating a high-velocity micrometeorite impacting environment, show that no solar wind hydrogen is needed to form $npFe^0$ and to change the optical spectra (Sasaki et al., 2001); (3) transmission electron microscopy (TEM) imaging has clearly shown that $npFe^0$ is present in the rim of nominally Fe-free minerals such as plagioclase (Keller and McKay, 1993; 1997; Wentworth et al., 1999).

One method to differentiate between the two formation processes is to use an isotopic tracer, as the two proposed mechanisms should impart different isotopic effects on $npFe^0$ in lunar regolith. In the solar wind hydrogen reduction scenario, the only possible source of Fe isotopic fractionation is the reduction of Fe(II) to Fe(0). As the solar wind hydrogen reduction process would have happened at high temperatures (i.e. $\sim$1500 K; Housley et al., 1973), and since equilibrium isotopic fractionation is proportional to $1/T^2$ as predicted by the classic equilibrium isotope fractionation theory (Urey, 1947), no measurable isotopic fractionation is expected. Recent theoretical calculations have shown no resolvable fractionation occurs between Fe metal and silicate/oxide at high temperatures (>1500 K), except in extremely high pressure environments, such as at the Earth's core-mantle boundary (Polyakov, 2009). Experimental work has also observed no equilibrium fractionation between Fe metal and silicate at high temperatures (Poitrasson et al., 2009). Therefore the Fe isotopic composition of the $npFe^0$ formed by solar wind hydrogen reduction would be expected to be unfractionated from the host lunar regolith. In the solar-wind-sputtering/micrometeorite-generated-vapor-deposit scenario (Hapke et al., 1975), kinetic effects could induce a preferential escape of the light isotopes of vaporized Fe to space. As a result, the remaining $npFe^0$ should be enriched in heavy isotopes relative to host lunar regolith. The Fe isotopic compositions of $npFe^0$ could therefore be used to distinguish which mechanism has dominated their formation.

Following this logic, Wiesli et al. (2003) and Moynier et al. (2006) both investigated the Fe isotopic compositions of bulk lunar regolith and found that it is enriched in the heavy isotopes of Fe when compared to lunar rocks by an average of 0.10‰/a.m.u. (atomic mass unit) and the most mature and finest lunar regolith samples have the most enriched heavy isotopes of Fe, up to 0.15‰/a.m.u. (Wiesli et al., 2003). Since the most mature and finest lunar regolith samples have the largest surface-to-volume ratio and have had more time to accumulate $npFe^0$, these investigations strongly suggest that the heavy-Fe-isotope-enrichment of the lunar regolith (relative to lunar rocks) is caused by the formation of $npFe^0$, which was predicted to have a highly fractionated Fe isotopic composition (more enriched in heavy isotopes of Fe than the bulk regolith). If these suggestions are correct, it would favor the impact-produced-vapor-deposit origin of the $npFe^0$. However, no direct isotopic investigation of the $npFe^0$ in the lunar regolith has been reported so far, due to its submicroscopic size (from a few to hundreds of nanometers; Hapke, 2001).

Plagioclase is a stoichiometrically Fe-free mineral (up to 0.25 wt% in bulk Apollo 16 regolith plagioclase; Bell and Mao, 1973; Taylor and Carter, 1973), so little intrinsic Fe from the host mineral could contaminate the $npFe^0$ on the surface. The Apollo 16 regolith is very mature (relatively determined by the amounts of $npFe^0$; Cirlin et al., 1974; Housley et al., 1975; Morris, 1976; Pearce et al., 1974), and hence contains large amounts of $npFe^0$ (Heiken et al., 1991). Thus Apollo 16 lunar regolith plagioclase mineral separates are ideal samples to search for the Fe isotopic composition of $npFe^0$. In order to access this $npFe^0$ signature, we used a step-by-step etching technique (Kitts et al., 2003), preferentially dissolving the surface (from 0.1 to 0.8 μm) of handpicked pure lunar regolith plagioclase grains with a series of weak acids. We have successfully managed to measure the Fe isotope signature of $npFe^0$ using Multi-Collector Inductively Coupled Plasma Mass Spectrometer (MC-ICP-MS). We will discuss the origin of the $npFe^0$ in lunar regolith from the perspective of Fe isotopic fractionation.

2. Material and methods

2.1. Sample treatment

We used the same sample solutions previously treated by Kitts et al. (2003). Here we briefly repeat the rationale and main steps (a detailed preparation procedures can be found in Kitts et al. (2003)). To maximize the proportion of nanophase Fe and limit the contamination from the intrinsic Fe of host minerals as much as possible, plagioclase from Apollo 16 regolith was chosen because (1) plagioclase stoichiometrically contains no Fe, and; (2) Apollo 16 regolith has long exposure ages and large surface-to-volume ratios (Heiken et al., 1991). Sample 60601 is from Apollo 16, station 10, 65 m southwest surface. Sample 62281 is from Apollo 16, station 2, south slope of Buster crater surface. For both samples, about 50 g of bulk regolith were used. First, the fine and ultra fine particles of the regolith were removed as suspensions using electronic grade methanol. The remaining material was initially size-sorted (35–75 μm and 75–150 μm), then the plagioclase grains were isolated, first using a Frantz magnetic separator and finally by hand. The handpicked clean plagioclase grains represent about 1.5–2.0% of the initial total mass of the regolith (Kitts et al., 2003).

The isolated plagioclase grains were first cleaned in MQ-e water (18.2 MΩ cm) in an ultrasonic bath for 60 s. The cleaned grains were then progressively etched by using 0.1 N HCl at room temperature. The first four etches (Etch1, 2, 3 and 4) each lasted for 1 h, while the final one (Etch5) continued for 20 h to consume as much sample as possible. The acid solution in each etching step was pipetted into cleaned PTFE beakers and used for the Fe purification. The Ca concentrations in the same solutions were previously measured by Kitts et al. (2003) and the etch depths were calculated therein (see Table 1). Each step was estimated to etch about 0.1 μm of sample (see Fig. 1; Kitts et al., 2003), which corresponds to the depth of the $npFe^0$ rim of plagioclase reported by Keller and McKay (1997).

2.2. Isotopic measurements

Prior to the mass spectrometry analysis, Fe was purified by ion exchange chromatography following procedures described previously

Table 1
Iron isotopic compositions of etched plagioclase in Apollo 16 lunar regolith (See the text for details of the δ and ε notation).

Sample	Treatment	Etch Depth[a]	$\delta^{56}Fe \pm 2SE$	$\delta^{57}Fe \pm 2SE$	$\delta^{58}Fe \pm 2SE$	$\varepsilon^{56}Fe$[b] 2SE	$\varepsilon^{58}Fe$[b] ± 2SE	$\varepsilon^{57}Fe$[c] ± 2SE	$\varepsilon^{58}Fe$[c] ± 2SE	n[d]
60601, 50 g, 35–75 um										
Etch2	0.1N HCl (1 h)	0.20	0.71 ± 0.05	1.05 ± 0.05	1.34 ± 0.12	0.11 ± 0.21	−0.39 ± 1.38	−0.16 ± 0.31	−0.61 ± 1.43	3
Etch3	0.1N HCl (1 h)	0.26	0.56 ± 0.10	0.88 ± 0.12	1.22 ± 0.31	−0.37 ± 0.23	0.56 ± 1.61	0.55 ± 0.34	1.29 ± 1.16	3
Etch4	0.1N HCl (1 h)	0.33	0.66 ± 0.12	1.00 ± 0.08	1.23 ± 0.03	−0.13 ± 0.65	−0.96 ± 1.12	0.19 ± 0.97	−0.71 ± 2.28	3
Etch5	0.1N HCl (20 h)	0.56	0.36 ± 0.25	0.60 ± 0.28	0.92 ± 0.22	−0.47 ± 0.67	1.25 ± 1.96	0.70 ± 0.99	2.18 ± 3.25	3
62281, 50 g, 35–75 um										
Etch1	0.1N HCl (1 h)	0.11	0.59 ± 0.04	0.94 ± 0.05	1.27 ± 0.12	−0.38 ± 0.17	0.24 ± 1.23	0.57 ± 0.26	0.99 ± 1.41	6
Etch2	0.1N HCl (1 h)	0.16	0.44 ± 0.11	0.71 ± 0.12	0.87 ± 0.11	−0.39 ± 0.35	−0.69 ± 1.03	0.57 ± 0.52	0.07 ± 1.57	6
Etch3	0.1N HCl (1 h)	0.22	0.57 ± 0.12	0.82 ± 0.11	0.98 ± 0.10	0.12 ± 0.42	−1.08 ± 0.98	−0.18 ± 0.62	−1.32 ± 1.70	6
Etch4	0.1N HCl (1 h)	0.28	0.49 ± 0.17	0.73 ± 0.17	0.83 ± 0.17	−0.01 ± 0.53	−1.35 ± 1.27	0.01 ± 0.80	−1.34 ± 2.21	6
Etch5	0.1N HCl (20 h)	0.45	0.22 ± 0.09	0.33 ± 0.09	0.20 ± 0.17	−0.01 ± 0.31	−2.31 ± 1.79	0.01 ± 0.47	−2.29 ± 1.81	5
62281, 50 g, 75–150 um										
Etch1	0.1N HCl (1 h)	0.13	0.48 ± 0.03	0.77 ± 0.03	0.83 ± 0.09	−0.40 ± 0.44	−1.86 ± 0.57	0.60 ± 0.66	−1.07 ± 1.44	2
Etch2	0.1N HCl (1 h)	0.20	0.56 ± 0.16	0.84 ± 0.15	1.13 ± 0.07	0.01 ± 0.59	0.20 ± 1.31	−0.01 ± 0.88	0.19 ± 2.47	2
Etch3	0.1N HCl (1 h)	0.33	0.51 ± 0.12	0.78 ± 0.11	1.06 ± 0.05	−0.19 ± 0.41	0.33 ± 1.01	0.28 ± 0.61	0.70 ± 1.82	2
Etch4	0.1N HCl (1 h)	0.44	0.39 ± 0.14	0.65 ± 0.16	0.92 ± 0.00	−0.53 ± 0.38	0.53 ± 2.02	0.78 ± 0.56	1.56 ± 2.76	2
Etch5	0.1N HCl (20 h)	0.73	0.29 ± 0.06	0.46 ± 0.08	0.68 ± 0.10	−0.23 ± 0.07	0.72 ± 0.03	0.34 ± 0.10	1.17 ± 0.10	2
Geostandard										
BCR-2	(Bulk)		0.07 ± 0.06	0.11 ± 0.06	0.01 ± 0.11	−0.05 ± 0.22	−1.40 ± 1.61	0.08 ± 0.32	−1.30 ± 1.99	4

[a] Etch depth is from Kitts et al. (2003) calculated from Ca concentration.
[b] $^{i}Fe/^{54}Fe$ normalized to $^{57}Fe/^{54}Fe = 0.362566$. $i = 56$ and 58 (Taylor et al., 1992).
[c] $^{i}Fe/^{54}Fe$ normalized to $^{56}Fe/^{54}Fe = 15.69786$. $i = 57$ and 58 (Taylor et al., 1992).
[d] Number of sample measurement.

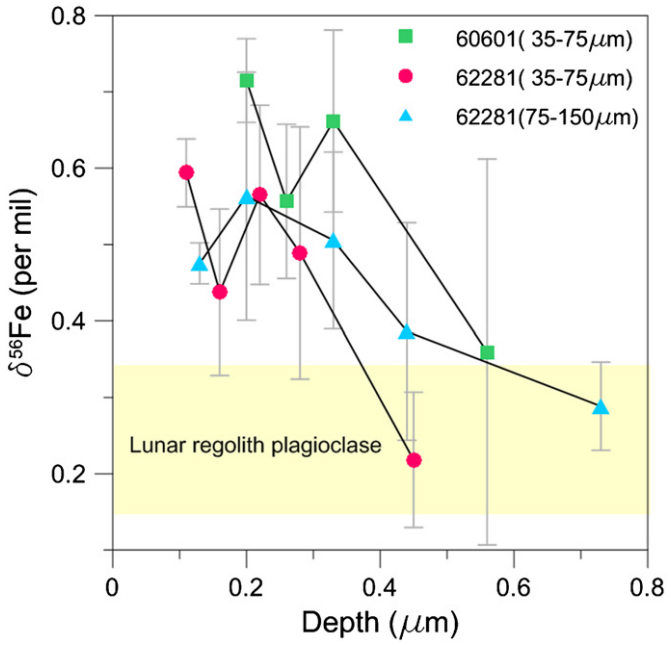

Fig. 1. Iron isotopic compositions expressed in delta notation ($\delta^{56}Fe$) relative to IRMM-014 vs. etching depth profile. Etching depth values are taken from Kitts (2003) derived from Ca concentrations. The yellow shaded area represents bulk plagioclase isotopic composition taken from lunar igneous rocks (Craddock et al., 2010). (For interpretation of the references to color in this figure legend, the reader is referred to the web version of this article.)

(Dauphas et al., 2004) and recently applied in Wang et al. (2011, 2012). Samples were dissolved in ~1 ml of 6 N HCl and loaded into columns filled with 1 mL AG1-X8 200–400 mesh anion-exchange resin. The matrix was first eluted in 8 mL (0.5+0.5+1+2+4 mL increments) of 6 M HCl and the Fe was collected in 9 mL (0.5+0.5+1+3+4 mL increments) of 0.4 M HCl. These purifications were repeated twice to ensure removal of all interfering isobars and other matrix elements. The Fe isotopic measurements were performed using a standard-sample bracketing method on the Thermo Scientific Neptune Plus Multi-Collector Inductively Coupled Plasma Mass Spectrometer (MC-ICP-MS) at Washington University in St. Louis, running at medium resolution (resolving power $M/\Delta M \sim 8500$). Both samples and standards were analyzed at the same concentration (0.5 ppm ± 10%) and were introduced into the MC-ICP-MS using a 100 μL/min PFA MicroFlow nebulizer and with an Apex-Q+Spiro desolvator, which reduces ambient species interferences and results in a higher machine sensitivity. The intensities of the isotopes ^{54}Fe, ^{56}Fe, ^{57}Fe and ^{58}Fe were measured in the L2, center, H1 and H2 Faraday cups respectively. Possible interferences from ^{54}Cr and ^{58}Ni were assessed by monitoring ^{53}Cr (L3) and ^{60}Ni (H4) respectively. The measurements were made on the flat-topped peak shoulder (light mass side) to avoid the interferences of $^{40}Ar^{14}N^{+}$, $^{40}Ar^{16}O^{+}$, $^{40}Ar^{14}OH^{+}$ and $^{40}Ar^{18}O^{+}$. The results are reported as delta notation relative to IRMM-014, where $\delta^{i}Fe = [(^{i}Fe/^{54}Fe)_{sample}/(^{i}Fe/^{54}Fe)_{IRMM-014} - 1] \times 10^{3}$, $i = 56$, 57 and 58. Because $\varepsilon^{53}Cr$ and $\varepsilon^{54}Cr$ anomalies were previously found in the same solutions (Kitts et al., 2003), it is necessary to check the non-mass fractionation effects for Fe isotopes too. For this reason, to correct the instrumental and natural mass-dependent fractionations, all the data were also normalized to $^{57}Fe/^{54}Fe = 0.362566$ or $^{56}Fe/^{54}Fe = 15.69786$ (Taylor et al., 1992) using the exponential law (Maréchal et al., 1999). The normalized data are reported in ε units, $\varepsilon^{i}Fe = [(^{i}Fe/^{54}Fe)_{sample}/(^{i}Fe/^{54}Fe)_{IRMM-014} - 1] \times 10^{4}$, $i = 56$, 57 and 58. The errors are reported as two standard errors (2SE) of the replicated measurements.

3. Results

The isotopic compositions of lunar regolith plagioclase etchings are presented in Table 1. For the three separate experiments (60601 35–75 μm; 62281, 35–75 μm and 75–150 μm), the first three/four one-hour etching solutions all have significantly higher $\delta^{56}Fe$ values

(δ^{56}Fe=0.39–0.71‰) than the last twenty-hour etching solutions (δ^{56}Fe=0.22–0.36‰). Fig. 1 shows a clear trend of δ^{56}Fe decreasing from the surface to the core of plagioclase grains for the three independent experiments. The δ^{56}Fe values in the last etching solution fall into normal lunar plagioclase values (δ^{56}Fe=0.15–0.34‰; shown as the yellow shaded area in Fig. 1; Craddock et al., 2010). The largest δ^{56}Fe offset from "average" lunar plagioclase Fe measured from surface etching is 0.71 $\pm$0.05‰, which we use as a possible end-member Fe isotopic composition of nanophase Fe, as discussed in the following section.

Because surface-related chromium isotopic anomalies have been previously found in the same etching solutions used in this study (Kitts et al., 2003), internally normalized Fe isotopic data for comparison, to check for non-mass dependent Fe isotopic signatures due to solar wind implantation (see Table 1 and Fig. 2). After correction for mass-dependent fractionation, either by normalizing to the ^{57}Fe/^{54}Fe or ^{56}Fe/^{54}Fe ratio, all ε^{56}Fe, ε^{57}Fe and ε^{58}Fe are equal to zero within analytical uncertainty. Unlike Cr isotopes there are no isotopic anomalies observed in Fe isotopes (see Fig. 2). Therefore, all the isotopic variations observed in our samples are caused by mass-dependent fractionation.

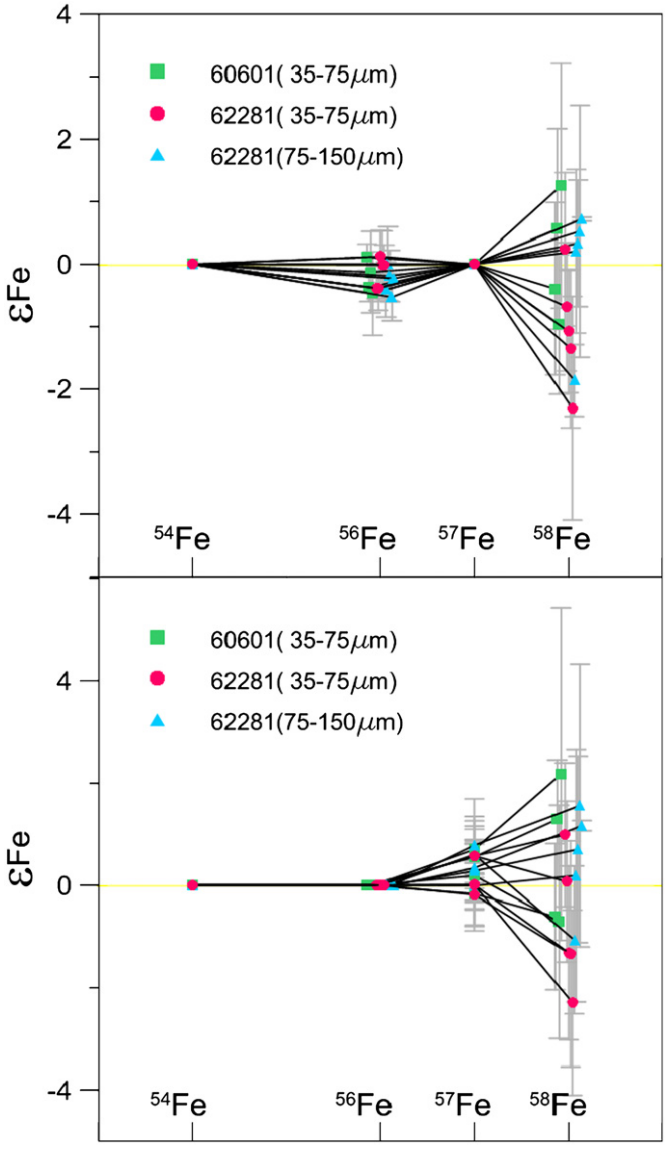

Fig. 2. Iron isotopic compositions expressed in epsilon notation (ε^{56}Fe) after mass-dependent fractionation corrections, either normalized to ^{57}Fe/^{54}Fe=0.362566 (Taylor et al., 1992; top panel) or to ^{56}Fe/^{54}Fe=15.69786 (Taylor et al., 1992; bottom panel) using the exponential law (Maréchal et al., 1999). Both sets of data show no Fe isotopic anomalies within analytical uncertainty.

4. Discussion

Plagioclase is a nominally Fe-free mineral, and in Apollo 16 regolith plagioclase the bulk Fe concentration is only 0.14–0.25 wt% (Bell and Mao, 1973; Taylor and Carter, 1973). The higher Fe concentration on the surface ($<$0.4 μm depth) of lunar regolith plagioclase implies that this extra Fe is probably not primary (Keller and McKay, 1997). Our study shows this secondary Fe has significant different isotopic compositions (δ^{56}Fe up to 0.71‰) from the host plagioclase (see Fig. 1). Three possible sources of this extrinsic Fe have been suggested: contamination by meteoritic components, solar wind Fe implantation or vapor-deposit Fe coating (Keller and McKay, 1997; Kitts et al., 2003).

Meteoritic components could contribute between 0.7% and 1.7% by mass in a typical regolith from Apollo 16 (Korotev, 1987). Meteorites, especially chondrites, usually contain high amounts of Fe–Ni metal (up to 20% in H group ordinary chondrites; Lodders and Fegley, 1998). However, no types of meteorites thus far measured for Fe isotopes could provide such heavy Fe isotopic compositions as measured here (δ^{56}Fe up to 0.71‰). For example, chondrites are the most frequent falls ($\sim$80%; Bevan et al., 1998) on the Earth (probably also on the Moon), and the average δ^{56}Fe is only 0.01 $\pm$0.01‰ (Craddock and Dauphas, 2011). Iron meteorites have higher δ^{56}Fe ($\sim$0.1‰; Poitrasson et al., 2005; Schoenberg and von Blanckenburg, 2006; Williams et al., 2006) but are still too light to provide the δ^{56}Fe=0.71‰ end-member required here. Achondrites, such as Martian, HED, or angrite, have various Fe isotopic compositions, but their δ^{56}Fe are all less than 0.2‰ (Anand et al., 2006; Poitrasson et al., 2004; Schoenberg and von Blanckenburg, 2006; Wang et al., 2012; Weyer et al., 2005). Thus, meteoritic components are not a plausible source for these highly fractionated Fe isotopic composition in the step etching solutions of the Apollo 16 lunar regolith plagioclase.

Solar wind is dominated by hydrogen and helium; heavy elements comprise less than 1% (Anders and Grevesse, 1989; Lodders, 2003). However, solar wind-derived implanted elements other than hydrogen and helium, such as noble gases (Benkert et al., 1993; Eberhardt et al., 1972), lithium (Chaussidon and Robert, 1999), carbon (Hashizume et al., 2004), nitrogen (Hashizume et al., 2000; Jull et al., 1995), and oxygen (Hashizume and Chaussidon, 2005; Ireland et al., 2006) have long been recognized at the surface of lunar regolith grains. Calculations based on solar wind flux shows that up to 0.3 wt% of the total Fe in lunar regolith could be implanted by solar wind (Shkuratov, 2012), which could therefore be a possible source for the secondary Fe found on the surface of lunar regolith plagioclase.

In addition, non-mass dependent Cr isotopic variations have been measured in the same etching used in our study. As with the heavy-Fe isotope-enriched etchings in this study, these anomalies were concentrated in the surface of lunar regolith plagioclases (Kitts et al., 2003). The origin of these Cr isotopic anomalies is still unclear, however, since these variations are definitively *non*-mass dependent, they can be best (if not only) explained by having formed by spallation in the solar atmosphere, transported to the Moon and implanted in lunar regolith by solar wind.

However, this conclusion based on Cr isotopes does not apply here for Fe, even though we have analyzed the same etching solutions. First, after correcting for mass dependent fractionation, within analytical uncertainty no *non*-mass dependent Fe isotopic

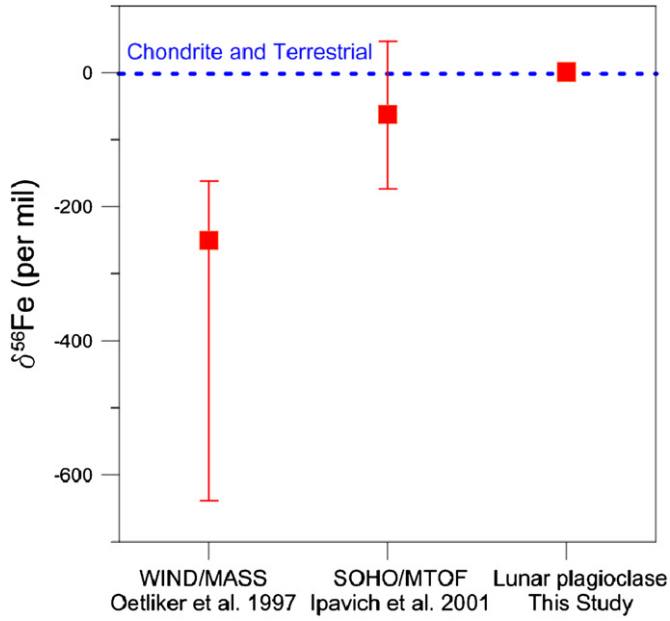

Fig. 3. Solar wind Fe isotopic compositions measured by spacecrafts (δ^{56}Fe) vs. Fe isotopic compositions measured in lunar regolith plagioclase surface etching solutions. The error bars for the literature data are 2σ; the error bar for this study is within the data symbol.

anomalies (ε^{56}Fe, ε^{57}Fe or ε^{58}Fe) are found (see Table 1 and Fig. 2). This does not necessarily exclude the possibilities of solar wind origin for the secondary Fe (e.g., if the Sun has a chondritic Fe isotopic composition) but is not definitive evidence for a solar wind origin. Second, inefficient Coulomb drag theory predicts heavier isotopes are depleted in solar wind relative to the outer convective zone (OCZ) of the Sun (Bochsler, 2000; Bodmer and Bochsler, 2000; Geiss et al., 1970; Wiens et al., 2004). This means that the implanted solar wind stable isotopic compositions should be enriched in light isotopes. Recent support for this theory comes from the isotopically light Mg isotopic composition (down to −2‰/a.m.u.) of solar wind collected by the Genesis mission (Humayun et al., 2011). For the Fe isotopic composition of solar wind, the High-Resolution Mass Spectrometer (MASS) loaded on the Wind spacecraft and the Mass Time-of-Flight Spectrometer (MTOF) on the Solar and Heliospheric Observatory (SOHO) spacecraft have reported very negative Fe isotopic compositions (see Fig. 3; Ipavich et al., 2001; Oetliker et al., 1997). The positive Fe isotopic compositions measured here (δ^{56}Fe up to 0.71‰) cannot therefore be attributed to solar wind implantation (see Fig. 3).

Lastly, abundant nanophase metallic Fe (npFe^0) has long been found in the vapor-deposit coating which universally covers mature lunar regolith particles like the Apollo 16 regolith plagioclase studied here (see Hapke, 2001 for a review). Previous acid leaching experiments have shown the surface npFe^0 can be readily accessed with short-term acid exposure (Gold et al., 1970; Hapke et al., 1970). The etching depth in this study (see Fig. 2; Kitts et al., 2003) is comparable with the appearance depth of the vapor-deposit npFe^0 observed by transmission electron microscope (Keller and McKay, 1993, 1997). This vapor-deposit Fe coating dominates the concentration of Fe on the rims of nominally Fe-free minerals such as plagioclase (Keller and McKay, 1997), hence controlling the Fe isotopic compositions measured in the surface etchings in this study. As such, the Fe of the surface (<0.4 μm) etching solutions of lunar Apollo 16 regolith plagioclases must represent the npFe^0 instead of meteorite components or solar wind implanted Fe.

In this study we directly show that heavier δ^{56}Fe is only concentrated in the topmost part (<0.4 μm) of lunar regolith plagioclase (see Fig. 1); the core has a "normal" δ^{56}Fe, comparable to that of plagioclase separated from lunar igneous rock (Craddock et al., 2010). We propose that the heavily enriched Fe isotopic compositions of the lunar regolith are solely caused by the formation of npFe^0, and that the degree of isotopic enrichment is determined by the amount of npFe^0 contained.

The highly fractionated Fe isotopic composition of npFe^0 measured in this study does not only explain why lunar regolith has a higher δ^{56}Fe than lunar igneous rock, but also sheds light on the origin of the npFe^0. As stated in the introduction, two competing formation mechanisms of npFe^0 (reduction of FeO in lunar regolith by solar wind vs. thermal disassociation with oxygen in solar wind sputtering/micrometeorite impact generated hot vapor) would have distinct Fe isotopic fractionation effects. As shown in Fig. 1 the npFe^0 measured here have highly fractionated heavy Fe isotopic composition (δ^{56}Fe up to 0.71‰), more than twice that of average lunar regolith (~0.3‰; Wiesli et al., 2003). This highly fractionated Fe isotopic composition of npFe^0 strongly disfavors the solar wind hydrogen reduction hypothesis. The fractionation can be best explained by the preferential loss of light Fe isotopes to space during the hot vaporization stage, as predicted by the classical thermal escape model (Wiesli et al., 2003).

Chemical fractionation between vapor deposits and source material during vapor transport has been previously reviewed in detail (Hapke et al., 1975; Hapke, 2001); here we will briefly discuss the possibility of isotopic fractionation. Following a classical thermal escape model (Jeans escape), atoms in the high-velocity-tail of the Maxwell–Boltzmann distribution may reach the planetary escape velocity and hence could be lost to space (Hunten, 1982; Jeans, 1925). Criss (1999) modeled the isotopic fractionation as a result of the preferential loss of lighter isotopes following this mechanism. The temperature of impact-produced vapor has been evaluated from both calculations and experiments (Anand et al., 2004; Cassidy and Hapke, 1975; Hapke et al., 1975; Tang et al., 2011; Yakovlev et al., 2011): depending on the natural variations of impact energy and source materials, the vapor temperature generally ranges from ~1500 to 3000 K or higher. At these high temperatures, a small but significant amount of Fe in the hot vapor would have velocity larger than the escape velocity of the Moon (2.38 km/s). As an example, at 2500 K (a reasonable vapor temperature) ~0.099% and ~0.077% of atoms of ^{54}Fe and ^{56}Fe respectively could be lost to space based on their different masses (see Fig. 4). These results were calculated using Eq. (1), after Criss (1999) (see Appendix for the equation derivation), as such:

$$\delta^{56}\mathrm{Fe}_{\mathrm{new}} = \frac{1-\sqrt{(2M^{56}/\pi \mathrm{RT})}V_e e^{-M^{56}V_e^2/(2\mathrm{RT})}+\mathrm{erf}\left(\sqrt{(2M^{56}/\pi \mathrm{RT})}V_e\right)}{1-\sqrt{(2M^{54}/\pi \mathrm{RT})}V_e e^{-M^{54}V_e^2/(2\mathrm{RT})}+\mathrm{erf}\left(\sqrt{(2M^{54}/\pi \mathrm{RT})}V_e\right)} \times(\delta^{56}\mathrm{Fe}_{\mathrm{source}}+1000)-1000 \quad (1)$$

where M^{54} is the mass of ^{54}Fe (kg/mol), M^{56} is the mass of ^{56}Fe (kg/mol), **R** is the gas constant (JK^{-1} mol^{-1}), V_e is the Lunar escape velocity (m/s) and T is the temperature of the vapor. Eq. (1) is plotted in Fig. 5 as a function of vapor temperature. The data range of the npFe^0 measured in the first etching solutions (0.48–0.71‰) is plotted as the shaded region in the diagram.

As shown in Fig. 5, the Fe isotope composition of npFe^0 in lunar plagioclase surface etchings can be explained as the condensation residue of material that has lost light Fe isotopes to space in a hot micrometeorite-impact-generated vapor (Hapke et al., 1975). The vapor temperature can be evaluated to between ~2500 and 2750 K if the fractionation starts from an average

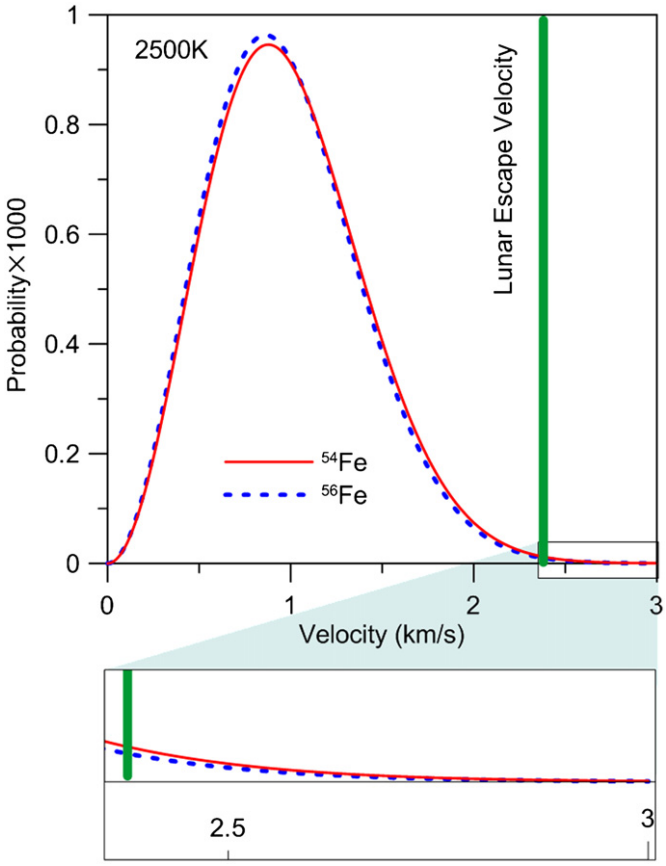

Fig. 4. Iron isotopic fractionation during thermal escape from the high-velocity-tail of Maxwell–Boltzmann distribution.

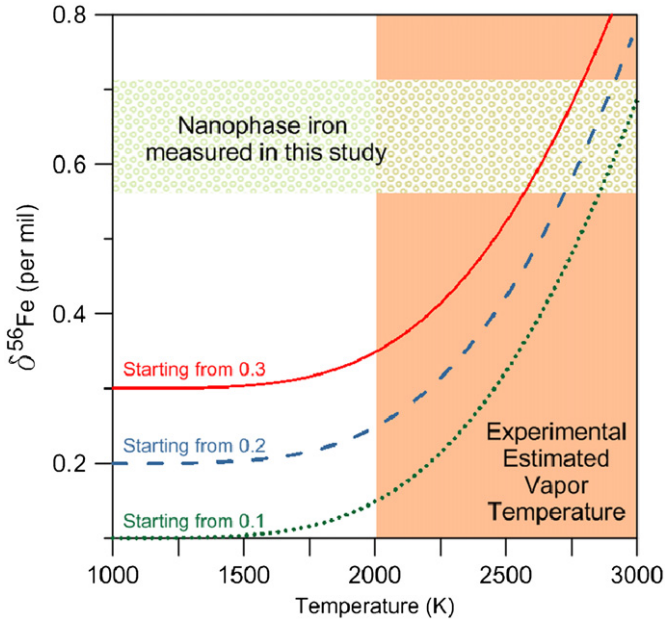

Fig. 5. The Fe isotopic compositions (δ^{56}Fe) of nanophase Fe measured in this study could be explained by fractionation during preferential thermal escape (see Eq. 1 in text) starting from a typical lunar regolith value (red solid line; δ^{56}Fe=0.3‰; Wiesli et al., 2003), a typical high-Ti lunar basalt value (blue dashed line; δ^{56}Fe=0.2‰; Liu et al., 2010; Poitrasson et al., 2004; Weyer et al., 2005) or a typical low-Ti lunar basalt/highland rock value (green dotted line; δ^{56}Fe=0.1‰; Liu et al., 2010; Poitrasson et al., 2004; Weyer et al., 2005). The experimentally estimated vapor temperature range is between ~2000 and 3000 K (Anand et al., 2004; Basu, 2005; Cassidy and Hapke, 1975; Hapke et al., 1975; Yakovlev et al., 2011).

lunar regolith Fe isotope composition (~0.3‰; Wiesli et al., 2003). It is worth noting that the average lunar regolith δ^{56}Fe already includes the influence of the high δ^{56}Fe caused by the formation of npFe^0. If the evaporating material has typical lunar igneous rock values (δ^{56}Fe=0.1−0.2‰; Liu et al., 2010; Poitrasson et al., 2004; Weyer et al., 2005; Wiesli et al., 2003), a higher temperature (~2750–3000 K) of the vapor is predicted. Considering the Fe isotope composition of npFe^0 from this stepwise etching experiment can only represent the lower limit value, we further suggest that a higher temperature (> 3000 K) is equally possible. These temperature estimates deduced from Eq. (1) (see Fig. 5) are compatible with the theoretical and experimental evaluations of the vapor temperature (~2000 to > 3000 K; Anand et al., 2004; Basu, 2005; Cassidy and Hapke, 1975; Hapke et al., 1975; Tang et al., 2011; Yakovlev et al., 2011).

The Fe isotope data presented here indicate that the formation of npFe^0 on the surface of lunar plagioclase is explained by the deposition of a solar wind sputtering/micrometeorite impact-generated vapor. Our results do not provide direct evidence for the origin of the npFe^0 found in lunar agglutinates (glassy breccias formed at the surface of the Moon by micrometeorite impacts) as, unfortunately, the stepwise etching method used in this study would dissolve much non-reduced Fe present in the agglutinate. Since the npFe^0 associated within agglutinates are larger than the npFe^0 found at the surface of regolith grains (Lucey et al., 2006), in-situ high precision measurements of Fe isotopes (e.g. Nano Secondary Ion Mass Spectrometry; Ong et al., 2012) might provide a solution to this problem in the future.

5. Conclusions

In this study, the Fe isotopic composition of nanophase metallic Fe (npFe^0) from the surface of lunar regolith plagioclase grains has been directly measured. The npFe^0 show large enrichments in the heaviest Fe isotopes (δ^{56}Fe up to 0.71‰) compared to lunar regolith (~0.3‰; Wiesli et al., 2003; Moynier et al. 2006) or lunar igneous rocks (0.1–0.2‰; Liu et al., 2010; Poitrasson et al., 2004; Weyer et al., 2005; Wiesli et al., 2003). These results provide good evidence that the enrichment in heavy Fe isotopes of the lunar regolith compared to lunar igneous rocks is the result of the presence of npFe^0 in the regolith. This conclusion is supported by previous studies on the bulk lunar regolith (Moynier et al., 2006; Wiesli et al., 2003). In addition, the highly fractionated Fe isotopic composition of npFe^0 measured here strongly favors a solar-wind-sputtering/micrometeorite-impact generated vapor deposit origin (Hapke et al., 1975), which is in agreement with the study of npFe^0 by Transmission Electron Microscopy (Keller and McKay, 1997). A thermal escape model predicts that preferential loss of light Fe isotopes to space in the hot vapor generated by constant solar wind sputtering/micrometeorite impacts can explain the Fe isotopic compositions of npFe^0. The temperature of the vapor can also be predicted from the model, and is inferred as between ~2750 and 3000 K. This is compatible with the temperature range proposed by previous theoretical or experimental studies (Anand et al., 2004; Cassidy and Hapke, 1975; Hapke et al., 1975; Tang et al., 2011; Yakovlev et al., 2011).

Acknowledgment

FM acknowledges the supports from the NASA LASER (NNX09AM64G); EXO (NNX12AD88G); and COSMO (NNX12AH70G) programs. KW thanks NASA for a PhD fellowship. KW thanks professor Robert Criss, Bradley Jolliff and Randy Korotev for

discussions. Paul Savage and Maxwell Thiemens are thanked for the language proof reading. Dr. Yang Liu and an anonymous reviewer are thanked for their thorough reviews, which greatly improved the quality of this manuscript. The editor, Dr. Tim Elliott, is also thanked for editing and handling this manuscript as well as for his comments.

Appendix A. Supporting information

Supplementary data associated with this article can be found in the online version at http://dx.doi.org/10.1016/j.epsl.2012.05.021.

References

Adams, J.B., Jones, R.L., 1970. Spectral reflectivity of lunar samples. Science 167, 737–739.
Anand, M., Russell, S.S., Blackhurst, R.L., Grady, M.M., 2006. Searching for signatures of life on Mars: an Fe-isotope perspective. Phil. Trans. R. Soc. B 361, 1715–1720.
Anand, M., Taylor, L.A., Nazarov, M.A., Shu, J., Mao, H.K., Hemley, R.J., 2004. Space weathering on airless planetary bodies: Clues from the lunar mineral hapkeite. Proc. Natl. Acad. Sci. USA 101, 6847–6851.
Anders, E., Grevesse, N., 1989. Abundances of the elements: meteoritic and solar. Geochim. Cosmochim. Acta 53, 197–214.
Basu, A., 2005. Nanophase Fe^0 in lunar soils. J. Earth Syst. Sci. 114, 375–380.
Bell, P.M., Mao, H.K., 1973. An analytical study of iron in plagioclase from Apollo 16 soils 64501, 64502, 64802, rock 66095 and Apollo 15 rock 15475. In: Proceedings of the Lunar Science Conference, vol. 4, pp. 57–59.
Benkert, J.-P., Baur, H., Signer, P., Wieler, R., 1993. He, Ne, and Ar from the solar wind and solar energetic particles in lunar ilmenites and pyroxenes. J. Geophys. Res. 98, 13147–13162.
Bevan, A.W.R., Bland, P.A., Jull, A.J.T., 1998. Meteorite flux on the Nullarbor Region, Australia, vol. 140. Geological Society, Special Publications, London, pp. 59–73.
Bochsler, P., 2000. Abundances and charge states of particles in the solar wind. Rev. Geophys. 38, 247–266.
Bodmer, R., Bochsler, P., 2000. Influence of Coulomb collisions on isotopic and elemental fractionation in the solar wind acceleration process. J. Geophys. Res. 105, 47–60.
Britt, D.T., Tholen, D.J., Bell, J.F., Pieters, C.M., 1992. Comparison of asteroid and meteorite spectra: Classification by principal component analysis. Icarus 99, 153–166.
Cassidy, W., Hapke, B., 1975. Effects of darkening processes on surfaces of airless bodies. Icarus 25, 371–383.
Chapman, C.R., 2004. Space weathering of asteroid surfaces. Annu. Rev. Earth Planet. Sci. 32, 539–567.
Chaussidon, M., Robert, F., 1999. Lithium nucleosynthesis in the Sun inferred from the solar-wind Li-7/Li-6 ratio. Nature 402, 270–273.
Cirlin, E.H., Housley, R.M., Goldberg, I.B., Paton, N.E., 1974. Ferromagnetic resonance as a method for studying regolith dynamics and breccia formation. In: Proceedings of the Lunar Science Conference, vol. 5, p. 121.
Clark, B.E., Hapke, B., Pieters, C., Britt, D., 2002. Asteroid space weathering and regolith evolution. In: Bottke, W.F., Cellino, A., Paolicchi, P., Binzel, R.P. (Eds.), Asteroids III. University of Arizona Press, Tucson, AZ, pp. 585–599.
Clark, R.N., 2009. Detection of adsorbed water and hydroxyl on the Moon. Science 326, 562–564.
Craddock, P.R., Dauphas, N., 2011. Iron isotopic compositions of geological reference materials and chondrites. Geostand. Geoanal. Res. 35, 101–123.
Craddock, P.R., Dauphas, N., Clayton, R.N., 2010. Mineralogical control on iron isotopic fractionation during lunar differentiation and magmatism. In: Proceedings of the Lunar and Planetary Science Conference, vol. 41, p. 1230.
Criss, R.E., 1999. Principles of Stable Isotope Distribution. Oxford University Press, New York.
Dauphas, N., Janney, P.E., Mendybaev, R.A., Wadhwa, M., Richter, F.M., Davis, A.M., van Zuilen, M., Hines, R., Foley, C.N., 2004. Chromatographic separation and multicollection-ICPMS analysis of iron. Investigating mass-dependent and -independent isotope effects. Anal. Chem. 76, 5855–5863.
Eberhardt, P., Geiss, J., Graf, H., Grögler, N., Mendia, M.D., Mörgeli, M., 1972. Trapped solar wind gases in lunar fines and a breccia. In: Proceedings of the Lunar and Planetary Science Conference, vol. 3, pp. 203–205.
Geiss, J., Hirt, P., Leutwyler, H., 1970. On acceleration and motion of ions in corona and solar wind. Sol. Phys. 12, 458–483.
Gold, T., Campbell, M.J., O'Leary, B.T., 1970. Optical and high-frequency electrical properties of the lunar sample. Science 167, 707–709.
Hapke, B., 1973. Darkening of silicate rock powders by solar wind sputtering. Moon 7, 342–355.
Hapke, B., 2001. Space weathering from Mercury to the asteroid belt. J. Geophys. Res. 106, 10039–10073.
Hapke, B., Cassidy, W., Wells, E., 1975. Effects of vapor-phase deposition processes on the optical, chemical, and magnetic properties of the lunar regolith. Moon 13, 339–353.
Hapke, B., Cohen, A.J., Cassidy, W.A., Wells, E.N., 1970. Solar radiation effects on the optical properties of Apollo 11 samples. In: Proceedings of the Lunar Science Conference, vol. 3, pp. 2199–2212.
Hashizume, K., Chaussidon, M., 2005. A non-terrestrial (16)O-rich isotopic composition for the protosolar nebula. Nature 434, 619–622.
Hashizume, K., Chaussidon, M., Marty, B., Robert, F., 2000. Solar wind record on the moon: Deciphering presolar from planetary nitrogen. Science 290, 1142–1145.
Hashizume, K., Chaussidon, M., Marty, B., Terada, K., 2004. Protosolar carbon isotopic composition: Implications for the origin of meteoritic organics. Astrophys. J. 600, 480–484.
Heiken, G., Vaniman, D., French, B.M., 1991. Lunar Sourcebook: A User's Guide to the Moon. Cambridge University Press.
Housley, R.M., Cirlin, E.H., Goldberg, I.B., Crowe, H., Weeks, R.A., Perhac, R., 1975. Ferromagnetic resonance as a method of studying the micrometeorite bombardment history of the lunar surface. In: Proceedings of the Lunar Science Conference, vol. 6, pp. 3173–3186.
Housley, R.M., Grant, R.W., Paton, N.E., 1973. Origin and characteristics of excess Fe metal in lunar glass welded aggregates. In: Proceedings of the Lunar Science Conference, vol. 4, pp. 2737–2749.
Humayun, M., Burnett, D.S., Jurewicz, A.J.G., 2011. Preliminary magnesium isotopic composition of solar wind from Genesis SOS. In: Proceedings of the Lunar and Planetary Science Conference, vol. 42, pp. 1211.
Hunten, D.M., 1982. Thermal and nonthermal escape mechanisms for terrestrial bodies. Planet. Space Sci. 30, 773–783.
Ipavich, F.M., Paquette, J.A., Bochsler, P., Lasley, S.E., Wurz, P., 2001. Solar wind iron isotopic abundances: results from SOHO/CELIAS/MTOF. in: AIP Conference Proceedings, vol. 598, pp. 121–126.
Ireland, T.R., Holden, P., Norman, M.D., Clarke, J., 2006. Isotopic enhancements of O-17 and O-18 from solar wind particles in the lunar regolith. Nature 440, 776–778.
Jeans, J.H., 1925. The Dynamical Theory of Gases. Cambridge University Press.
Jull, A.J.T., Lal, D., Donahue, D.J., 1995. Evidence for a non-cosmogenic implanted C-14 component in lunar samples. Earth Planet. Sci. Lett. 136, 693–702.
Keller, L.P., McKay, D.S., 1993. Discovery of vapor deposits in the lunar regolith. Science 261, 1305–1307.
Keller, L.P., McKay, D.S., 1997. The nature and origin of rims on lunar soil grains. Geochim. Cosmochim. Acta 61, 2331–2341.
Kitts, B.K., Podosek, F.A., Nichols, R.H., Brannon, J.C., Ramezani, J., Korotev, R.L., Jolliff, B.L., 2003. Isotopic composition of surface-correlated chromium in Apollo 16 lunar soils. Geochim. Cosmochim. Acta 67, 4881–4893.
Korotev, R.L., 1987. The nature of the meteoritic components of Apollo 16 soil, as inferred from correlations of iron, cobalt, iridium, and gold with nickel. J. Geophys. Res. 92, E447–E461.
Liu, Y., Guan, Y., Zhang, Y., Rossman, G.R., Eiler, J.M., Taylor, L.A., 2012. Lunar surface water in agglutinates: origin and abundances. In: Proceedings of the Lunar and Planetary Science Conference, vol. 43.
Liu, Y., Spicuzza, M.J., Craddock, P.R., Day, J.M.D., Valley, J.W., Dauphas, N., Taylor, L.A., 2010. Oxygen and iron isotope constraints on near-surface fractionation effects and the composition of lunar mare basalt source regions. Geochim. Cosmochim. Acta 74, 6249–6262.
Lodders, K., 2003. Solar system abundances and condensation temperatures of the elements. Astrophys. J. 591, 1220–1247.
Lodders, K., Fegley, B., 1998. The Planetary Scientist's Companion. Oxford University Press, New York.
Lucey, P., Korotev, R.L., Gillis, J.J., Taylor, L.A., Lawrence, D., Campbell, B.A., Elphic, R., Feldman, B., Hood, L.L., Hunten, D., Mendillo, M., Noble, S., Papike, J.J., Reedy, R.C., Lawson, S., Prettyman, T., Gasnault, O., Maurice, S., 2006. Understanding the lunar surface and space-moon interactions. Rev. Mineral. Geochem. 60, 83–219.
Maréchal, C.N., Télouk, P., Albarède, F., 1999. Precise analysis of copper and zinc isotopic compositions by plasma-source mass spectrometry. Chem. Geol. 156, 251–273.
Moroz, L.V., Fisenko, A.V., Semjonova, L.F., Pieters, C.M., Korotaeva, N.N., 1996. Optical effects of regolith processes on S-asteroids as simulated by laser shots on ordinary chondrite and other mafic materials. Icarus 122, 366–382.
Morris, R.V., 1976. Surface exposure indices of lunar soils: a comparative FMR study. In: Proceedings of the Lunar Science Conference, vol. 7, pp. 315–335.
Moynier, F., Albarède, F., Herzog, G.F., 2006. Isotopic composition of zinc, copper, and iron in lunar samples. Geochim. Cosmochim. Acta 70, 6103–6117.
Oetliker, M., Hovestadt, D., Klecker, B., Collier, M.R., Gloeckler, G., Hamilton, D.C., Ipavich, F.M., Bochsler, P., Managadze, G.G., 1997. The isotopic composition of iron in the solar wind: first measurements with the MASS sensor on the Wind spacecraft. Astrophys. J. 474, L69.
Ong, W.J., Floss, C., Gyngard, F., 2012. Negative secondary ion measurements of 54Fe/56Fe and 57Fe/56Fe in presolar silicate grains from Acfer 094. In: Proceedings of the Lunar and Planetary Science Conference, vol. 43, p. 1864.
Pearce, G.W., Strangway, D.W., Gose, W.A., 1974. Magnetic properties of Apollo samples and implications for regolith formation. In: Proceedings of the Lunar Science Conference, vol. 5, pp. 2815–2826.
Pieters, C.M., Goswami, J.N., Clark, R.N., Annadurai, M., Boardman, J., Buratti, B., Combe, J.P., Dyar, M.D., Green, R., Head, J.W., Hibbitts, C., Hicks, M., Isaacson, P., Klima, R., Kramer, G., Kumar, S., Livo, E., Lundeen, S., Malaret, E., McCord, T., Mustard, J., Nettles, J., Petro, N., Runyon, C., Staid, M., Sunshine, J., Taylor, L.A.,

Tompkins, Y., Varanasi, P., 2009. Character and spatial distribution of OH/H_2O on the surface of the Moon seen by M3 on Chandrayaan-1. Science 326, 568–572.
Pieters, C.M., Taylor, L.A., Noble, S.K., Keller, L.P., Hapke, B., Morris, R.V., Allen, C.C., McKay, D.S., Wentworth, S., 2000. Space weathering on airless bodies: resolving a mystery with lunar samples. Meteorit. Planet. Sci. 35, 1101–1107.
Poitrasson, F., Halliday, A.N., Lee, D.C., Levasseur, S., Teutsch, N., 2004. Iron isotope differences between Earth, Moon, Mars and Vesta as possible records of contrasted accretion mechanisms. Earth Planet. Sci. Lett. 223, 253–266.
Poitrasson, F., Levasseur, S., Teutsch, N., 2005. Significance of iron isotope mineral fractionation in pallasites and iron meteorites for the core-mantle differentiation of terrestrial planets. Earth Planet. Sci. Lett. 234, 151–164.
Poitrasson, F., Roskosz, M., Corgne, A., 2009. No iron isotope fractionation between molten alloys and silicate melt to 2000 degrees C and 7.7 GPa: experimental evidence and implications for planetary differentiation and accretion. Earth Planet. Sci. Lett. 278, 376–385.
Polyakov, V.B., 2009. Equilibrium iron isotope fractionation at core-mantle boundary conditions. Science 323, 912–914.
Sasaki, S., Nakamura, K., Hamabe, Y., Kurahashi, E., Hiroi, T., 2001. Production of iron nanoparticles by laser irradiation in a simulation of lunar-like space weathering. Nature 410, 555–557.
Schoenberg, R., von Blanckenburg, F., 2006. Modes of planetary-scale Fe isotope fractionation. Earth Planet. Sci. Lett. 252, 342–359.
Shkuratov, Y.G., 2012. Forgotten solar-wind iron implanted in lunar regolith. In: Proceedings of the Lunar and Planetary Science Conference, vol. 43, p. 1286.
Sunshine, J.M., Farnham, T.L., Feaga, L.M., Groussin, O., Merlin, F., Milliken, R.E., A'Hearn, M.F., 2009. Temporal and spatial variability of lunar hydration as observed by the Deep Impact spacecraft. Science 326, 565–568.
Tang, H., Wang, S., Li, X., 2011. Simulation of nanophase iron production in lunar space weathering. Planet. Space Sci. 60, 322–327.
Taylor, H.C.J., Carter, J.L., 1973. Silicate mineral chemistry of Apollo soils 15411, 15501, 66081, and 69941. In: Proceedings of the Lunar Science Conference, vol. 4, pp. 291–307.
Taylor, L.A., Pieters, C.M., Keller, L.P., Morris, R.V., McKay, D.S., 2001. Lunar mare soils: space weathering and the major effects of surface-correlated nanophase Fe. J. Geophys. Res. 106, 27985–27999.
Taylor, L.A., Rossman, G.R., Qi, Q., 1995. Where has all the lunar water gone? In: Proceedings of the Lunar and Planetary Science Conference, vol. 26, pp. 1399–1400.
Taylor, P.D.P., Maeck, R., De Bièvre, P., 1992. Determination of the absolute isotopic composition and atomic weight of a reference sample of natural iron. Int. J. Mass Spectrom. Ion Processes 121, 111–125.
Urey, H.C., 1947. The thermodynamic properties of isotopic substances. J. Chem. Soc., 562–581.
Wang, K., Moynier, F., Dauphas, N., Barrat, J.-A., Craddock, P., Sio, C.K., 2012. Iron isotope fractionation in planetary crusts. Geochim. Cosmochim. Acta 89, 31–45.
Wang, K., Moynier, F., Podosek, F., Foriel, J., 2011. ^{58}Fe and ^{54}Cr in early solar system materials. Astrophys. J. Lett. 739, L58.
Wentworth, S.J., Keller, L.P., McKay, D.S., Morris, R.V., 1999. Space weathering on the Moon: Patina on Apollo 17 samples 75075 and 76015. Meteorit. Planet. Sci. 34, 593–603.
Weyer, S., Anbar, A.D., Brey, G.P., Munker, C., Mezger, K., Woodland, A.B., 2005. Iron isotope fractionation during planetary differentiation. Earth Planet. Sci. Lett. 240, 251–264.
Wiens, R.C., Bochsler, P., Burnett, D.S., Wimmer-Schweingruber, R.F., 2004. Solar and solar-wind isotopic compositions. Earth Planet. Sci. Lett. 222, 697–712.
Wiesli, R.A., Beard, B.L., Taylor, L.A., Johnson, C.M., 2003. Space weathering processes on airless bodies: Fe isotope fractionation in the lunar regolith. Earth Planet. Sci. Lett. 216, 457–465.
Williams, H.M., Markowski, A., Quitte, G., Halliday, A.N., Teutsch, N., Levasseur, S., 2006. Fe isotope fractionation in iron meteorites: New insights into metal-sulphide segregation and planetary accretion. Earth Planet. Sci. Lett. 250, 486–500.
Yakovlev, O., Gerasimov, M., Dikov, Y., 2011. Conditions of condensate rim formation on the surface of lunar regolith particles. Geochem. Int. 49, 967–973.